PROCEEDINGS, 48th Workshop on Geothermal Reservoir Engineering
Stanford University, Stanford, California, February 6-8, 2023
SGP-TR-224

Spatial Prediction for Bottom Hole Temperature and Geothermal Gradient in Colombia

Jhon Camilo Matiz-León

Servicio Geológico Colombiano – SGC

Dg 53 No. 34-53

jmatiz@sgc.gov.co

Keywords: geothermal gradient, sedimentary basins, BHT, geostatistical simulation 3D, interpolation, spatial prediction.

ABSTRACT

The estimation of the geothermal potential of sedimentary basins becomes an essential condition through the representation of temperature and its depth variations. Part of the improvement in the accuracy of the variables of temperature and geothermal gradient (GG) lies in the estimation of the possible values through robust statistics, while knowing their positions in space. The processing and representation environments used for the spatial prediction correspond to 2D and 3D. The exploratory and structural analysis of data was performed using the statistical computing environment R. 2D modeling was executed in Oasis Montaj by Geosoft with pixels as the minimum representation unit. 3D modeling was implemented in GeoModeller by Intrepid Geophysics, using the voxel in the representation of 3D models as a volumetric unit. The techniques used for the 2D and 3D modeling are framed in the deterministic methods (minimum curvature and Inverse Weighted Distance – IDW method), probabilistic methods with Ordinary Kriging, and geostatistical simulation with Sequential Gaussian Simulation (SGS). The analysis was applied in three sedimentary basins with Bottom Hole Temperatures (BHT) values of hydrocarbon wells and was based on a spatial datum known by the observer.

1. INTRODUCTION

The deterministic and probabilistic spatial prediction methods have been defined as a procedure that allows calculating the value of a variable and its position in space (Ramírez, 2010), from sampled values of the same variable in other positions of the space, by means of mathematical algorithms that facilitate the calculation of them (Deutsch, 2002). The most common geostatistical methods from a set of irregularly distributed points can be classified into global and local interpolators, where the former is characterized by using all the data from the study area to generate predictions through smoothing functions that reveal areas of greater deviation from the general trend (Webster and Oliver, 2007). Local interpolators, on the other hand, are characterized by working around the point to interpolate as long as there is a correlation in the surface, which will decrease while the distance between the points sampled to the point to be interpolated is greater. Kriging is the most representative method of this type of interpolation (Webster and Oliver, 2007)

2. MATERIALS

2.1 Bottom Hole Temperature Wells

For the calculation of the apparent geothermal gradient, the LogDB database is available, which was used to compile pairs of temperature and depth data for the 3303 wells drilled (Alfaro et al., 2009). In Figure 1, the location of the wells with temperatures located in the three sedimentary basins under study is observed (Barrero et al., 2007). The LogDB database is located in the Exploration and Production Information Service (EPIS), system belonging to the Petroleum Information Bank (BIP), currently administered and property of the Colombian Geological Survey (SGC). The compilation of information and the structuring and processing of raw data was generated by the Geothermal Resources Research and Exploration Group of the SGC (Alfaro et al., 2009). In the estimation of the coefficients to apply the topographic correction to the geothermal gradient (Westaway and Younger, 2014), the Digital Elevation Model (DEM) of Shuttle Radar Topography Mission (SRTM) with a resolution of 30 m was used, which is shown in Figure 1 (Farr et al., 2007).

2.2 Geothermal Gradient

With topographically corrected geothermal gradient data, spatial prediction interpolations were generated. Table 1 shows the statistics of the observed geothermal gradient ranges, depths of the bottom of the well and the distances (in kilometers) of the BHT wells (Deming, 1989) located in the three sedimentary basins under study (Alfaro et al., 2010). Although a difference is indicated with the location of the wells, with a minimum distance of 0.001 km and a maximum of 746.29 km between wells, this being a difficulty in the elaboration of spatial prediction models, consideration is given to the technical characteristics and economic conditions that the realization of a BHT perforation is required for its subsequent spatial prediction (Alfaro et al., 2015).

Table 1: Well distribution with the calculation of the geothermal gradient by sedimentary basin and depth ranges.

Sedimentary Basin	Total Wells	Geothermal Gradient Range	Depth Range	Average distance between wells	Minimum distance between wells	Maximum distance between wells
Magdalena Middle Valley	2330	3.41°C/km – 63.19°C/km	500 m – 4816 m	208.82 km	0.001 km	599.76 km
Eastern Cordillera	112	11.03°C/km – 69.83°C/km	568 m – 5823 m	119.37 km	0.00449 km	439.46 km
Eastern Plains	861	5.007°C/km – 57.61°C/km	515 m – 6273 m	76.726 km	0.00011 km	445.69 km
Total	3303	3.41°C/km – 69.83°C/km	500 m – 6273 m	197.32 km	0.001 km	746.29 km

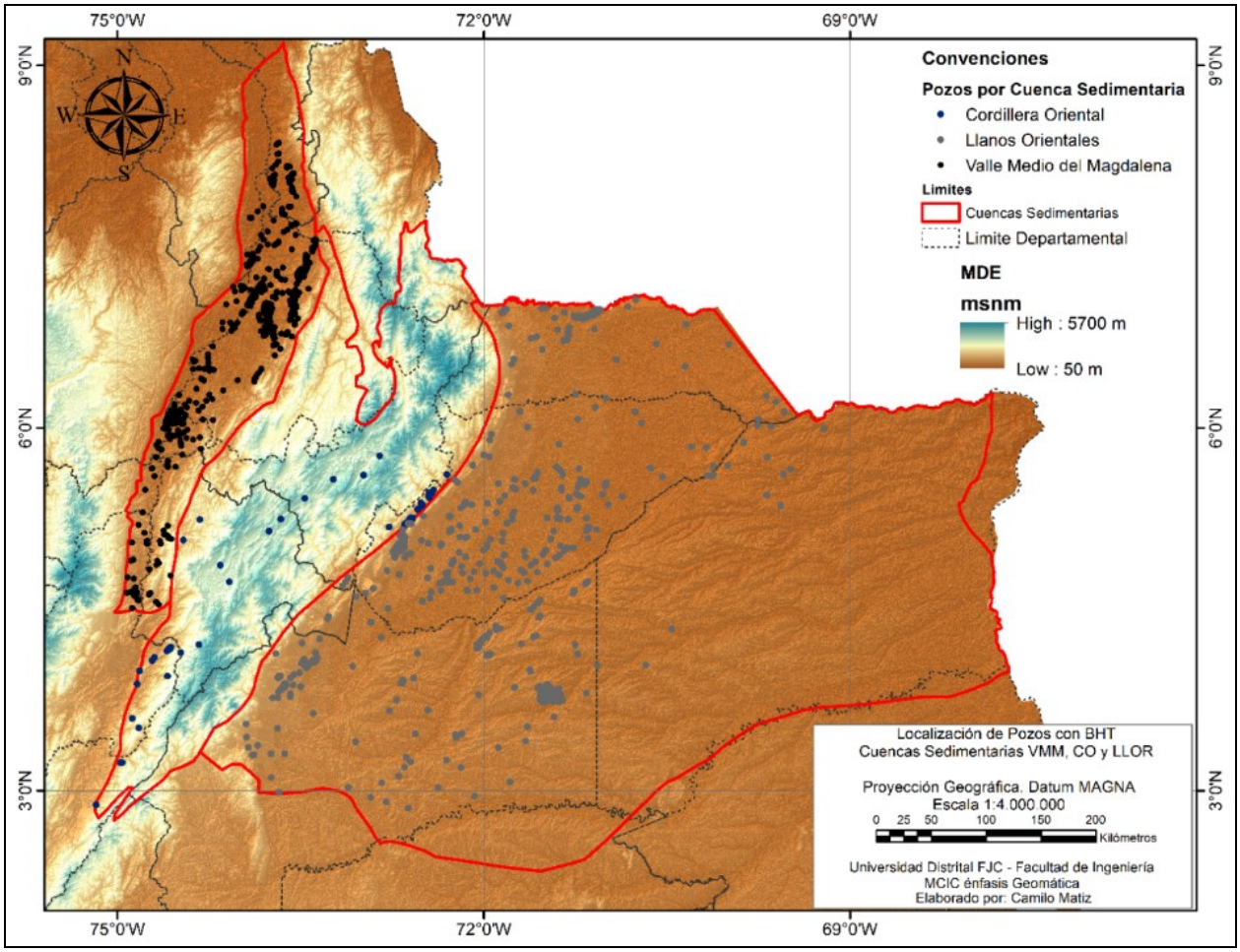

Figure 1: Digital elevation model and spatial distribution of BHTs.

3. METHODS

The methods used in the development of spatial prediction models (Fortin and Dale, 2005) were carried out in two processing and representation environments: 2D and 3D. 2D modeling was executed in Geosoft's Oasis Montaj software and 3D modeling was implemented in GeoModeller by Intrepid Geophysics. The statistics used for the 2D and 3D modeling are centered in the deterministic methods of minimum curvature and IDW (Álvarez et al., 2011). Probabilistic methods were completed using Kriging (exploratory analysis, structural analysis, and cross-validation) and geostatistical simulation with the Sequential Gaussian Simulation (SGS) method (Amezcua and Van Leeuwen, 2014). The methods are framed in the characterization of the prediction models using pixels as the minimum representation unit for 2D, and the voxel as a volumetric unit in the representation of 3D models.

3.1 Exploratory Analysis

In the exploratory analysis, descriptive measures were applied: central tendency (mean and median), amplitude (minimum and maximum), dispersion (standard deviation, variance and coefficient of variation) and structure (skewness and kurtosis). Graphical analysis included histograms, quantile-quantile diagrams, and the elimination of atypical data (Haining, 2004). The exploratory and structural analysis of the data was carried out in the statistical software R, which is open source. The specific packages used in the exploratory analysis correspond to sjstats, e1071, psych, sjPlot, lattice, caret, outliers, and ggplot2. For the structural analysis (semivariograms), the packages used correspond to sp, car, maptools, gstat, geoR, rgdal and spatstat.

3.1.1 Descriptive Statistics

The central tendency measures highlight the absence or not of normality in the data. The median/mean relation, which should tend to 1 in normal distributions, is 0.9183 for BHTs. The median/mean of the GG is 0.8832. These relationships allow to state that the data does not have a normal distribution. Additionally, there is a possibility for outliers, which is also highlighted by the range of observations in each of the variables. The measures of central tendency for the BHT and GG can be observed in Table 2.

Table 2: Descriptive measures for the BHT and GG.

Analysis	Measure	BHT	GG
Central Tendency	Mean	73.75229	26.062
	Median	67.73136	23.02062
Amplitude	Minimum	38.11291	6.866284
	Maximum	193.7427	214.36
Scale	Standard Deviation	22.53367	11.35423
	Variance	507.7661	128.9186
	Coefficient of Variation	30.55318%	43.56623%
Structure	Asymmetry Coefficient	1.109923	5.536042
	Kurtosis	1.134615	60.68424

3.2 Graphical Analysis

The histograms and box diagrams of BHT and GG presented in Figure 2 and Figure 3, respectively, certify the presence of high values of low frequency, and the wide grouping of lower values of temperature with high frequencies. The quantile - quantile diagrams show the concavities of the straight lines at the ends of each, confirming the asymmetric distribution to the right. Where the observations touch the line, a behavior parallel to it is evident, marking a certain homogeneity towards the central measurements of the temperatures. For the GG, the graphical analysis was more forceful when exposing a very marked heterogeneity of the observations. A large number of observations with high values of GG, but with few representations or frequencies, and asymmetry to the right and the consp icuous concavity of the data in the quantile-quantile diagrams confirm the presence of extreme values that affect the normality of the data.

3.2.1 Removing Outliers

Although the exploratory analysis of both the BHT and GG data corroborates the existence of extreme values for both variables, the observations away from the centrality of the data do not necessarily correspond to an outlier. Geologically one must take into account the composition of a sedimentary basin, generally composed of sandstones, shales, limestones, and granites in depth (Figure 4) (Balling et al., 1981).

3.3 Data Transformation

When examining the data through exploratory analysis, some tendency of the natural logarithm function (lognormal) was observed in the observations of BHT, but being more noticeable for GG observations. In the BHT values, the transformation of the observations was applied to the total data set. The transformation of the GG data to a natural logarithmic distribution was applied after the elimination of outliers to avoid the variability of the total set of observations. For the BHT, an improvement in the normal distribution of the data was found. The transformation to natural logarithm allowed the variables to improve the distribution of the observations. However, in the Quantile-Quantile diagrams, a separation of extreme data in relation to the distribution trend line is observed. This reflects that in its entirety, the observations do not correspond to an entirely lognormal distribution. The graphics results that were obtained for the BHT are presented in Figure 5 and for GG are show in Figure 6.

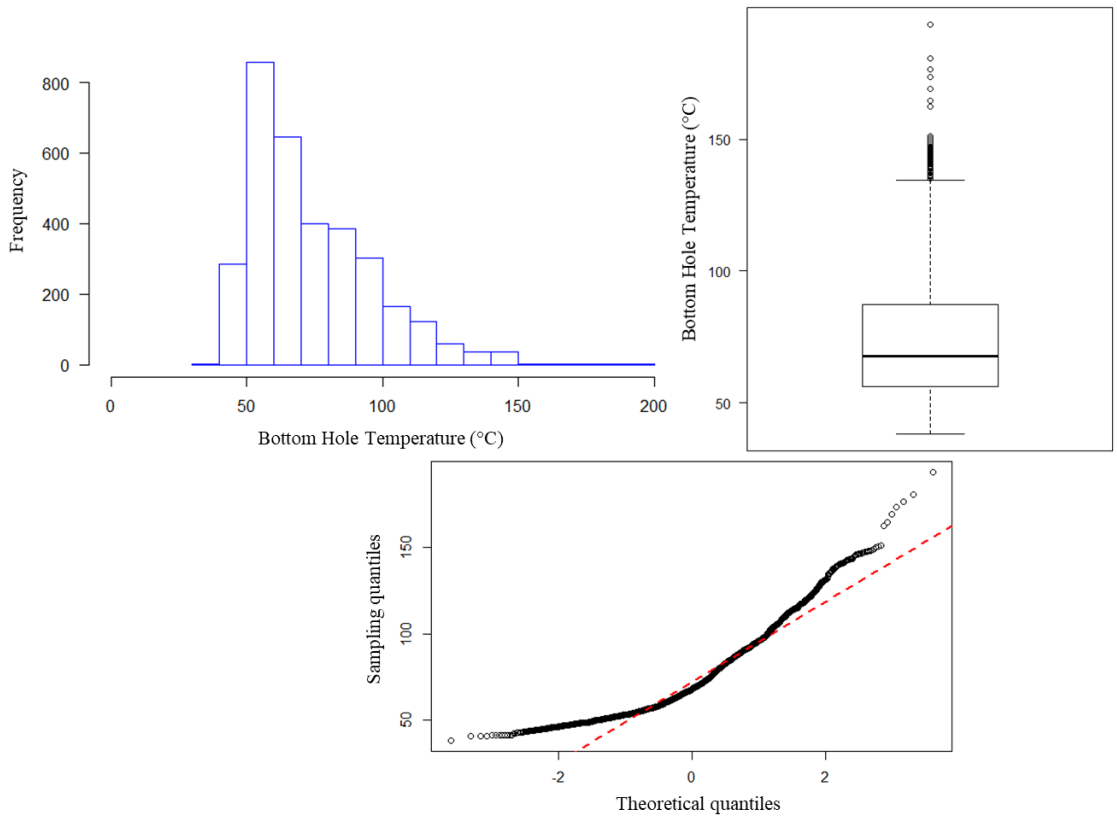

Figure 2: Histogram, boxplot, and quantile-quantile graphics for BHT.

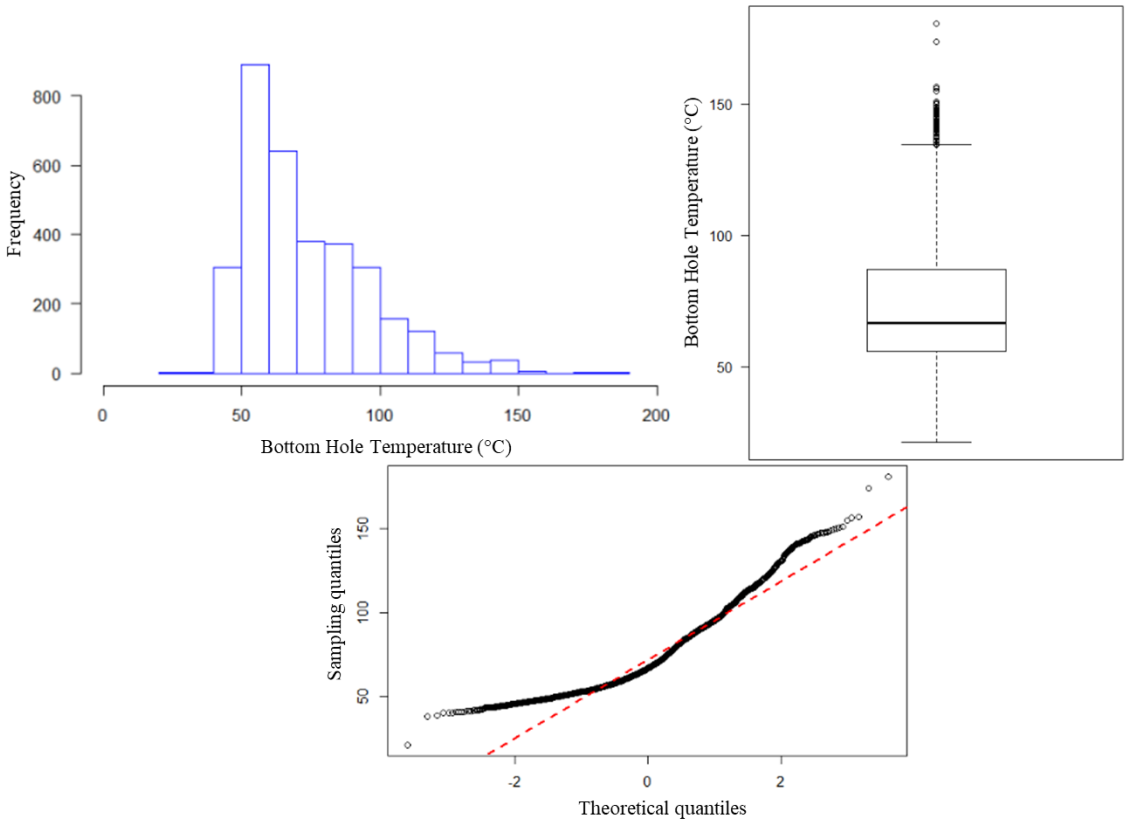

Figure 3: Histogram, boxplot, and quantile-quantile graphics for GG.

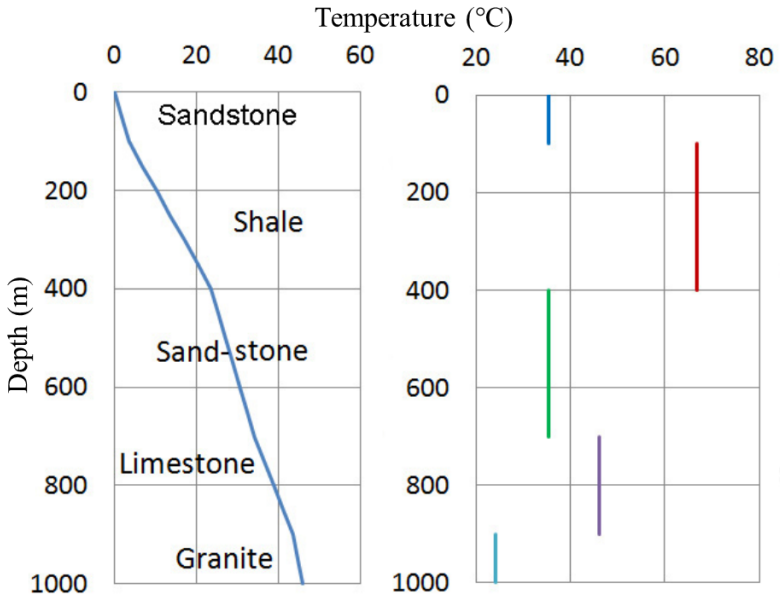

Figure 4: Generic relationship of temperature as a function of depth for lithologies in sedimentary basins, illustrating changes in geothermal gradient by lithology (Morgan & Scott, 2014).

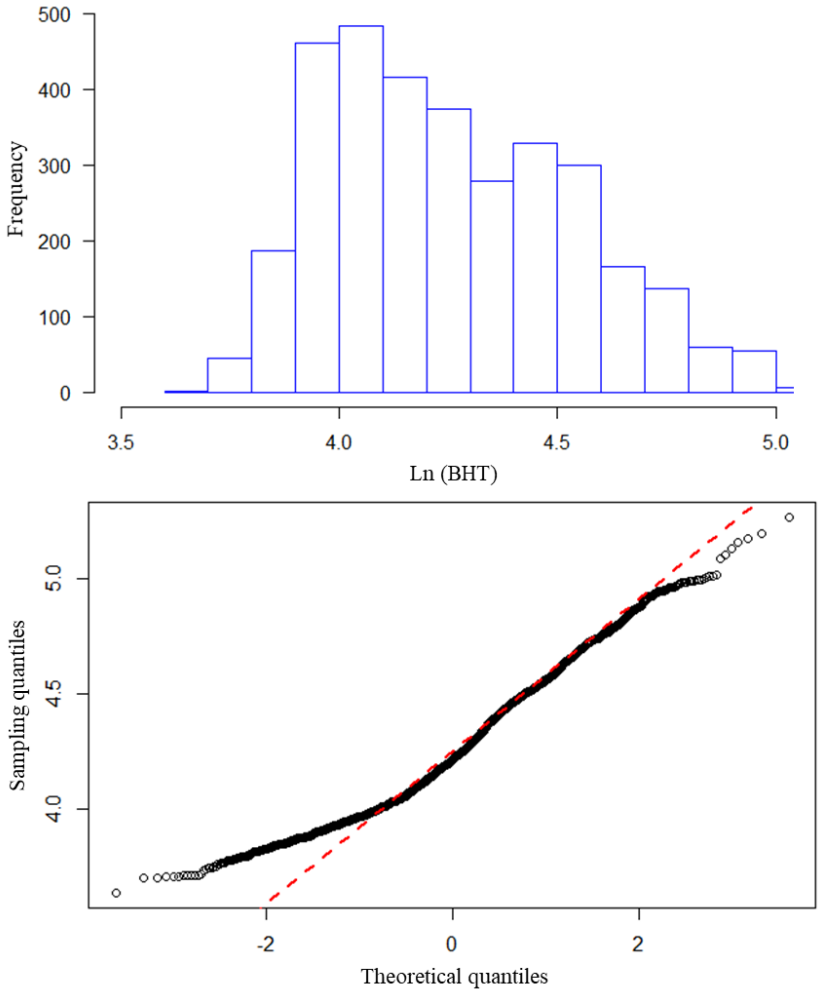

Figure 5: Histogram without outliers, transformed to a lognormal distribution, and quantile-quantile diagram for BHT.

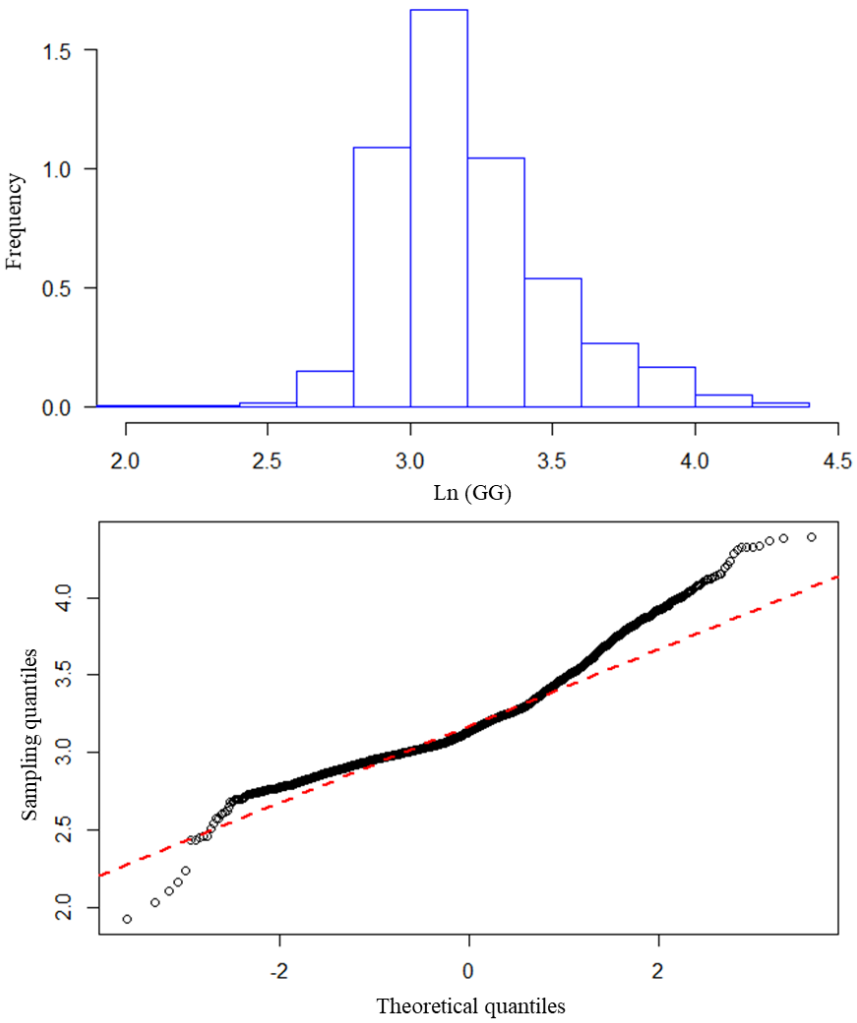

Figure 6: Histogram without outliers, transformed to a lognormal distribution, and quantile-quantile diagram for GG.

3.4 Structural Analysis

In the analysis of the structure of the observations, to quantify the best (between greater or lesser) similarity that exists between pairs of data, the moments of order 2 are considered as the main source of contribution in the elementary and operational description of the continuity space. This characterization is carried out by means of variograms to the variable to be spatially predicted. In the structural evaluation of the BHT and GG data, the experimental variograms of the variables, the behavior of the anisotropy, the correlation of the adjustable theoretical variograms to the observations, and the validation of the obtained model were represented.

3.4.1 Experimental Variogram

The estimated experimental variogram corresponds to the global or omnidirectional variogram, which depends not only on the direction (angular tolerance of 90°) but also on the magnitude of semivariance in relation to distance. Table 3 lists the parameters with which the experimental variograms were estimated for the BHT and GG. These parameters were tested with a trial and error processes, and it was determined to take the same parameters to see the behavior of the BHT and GG models under the same conditions of spatial variability.

Table 3: Descriptive measures for semivariogram analysis of the BHT and GG.

Analysis	BHT	GG
Central Tendency	90° omnidirectional	90° omnidirectional
Steps numbers (Lag)	10	10
Step size (Lag)	25000 m	25000 m

Trend	Constant	Constant
Estimator	Classic	Classic

The experimental variograms (mean and variogram cloud) calculated for the BHT are shown in Figure 7. The resulting mean variograms allow observing that the relative variance $\hat{\gamma}(h)$ contains fluctuations (due to very high differences in values) when the spatial separation distance increases. The great distances contained for the data are derived from the geological – geophysical analysis that must be taken into account for the drilling of hydrocarbon production wells. Drilling should be carried out in sedimentary basins, such as those under study and not in areas of igneous or volcanic origin, where there is no access to the petroleum resource in the country. In turn, the variograms show that the behavior at the origin is discontinuous, presenting a generalized so-called nugget effect in the variance. For the BHT, the sill does not stabilize while the distance increases, so there is no definitive range. This absence of sill is observed because the observation scale corresponds to one third of the maximum distance reached in the variogram. The analysis of the variogram clouds shows the spatial variability of the observations for the BHT. This indicates that pairs of observations are responsible for high values, indicating the strong presence of atypical data evidencing the different data from their close neighbors.

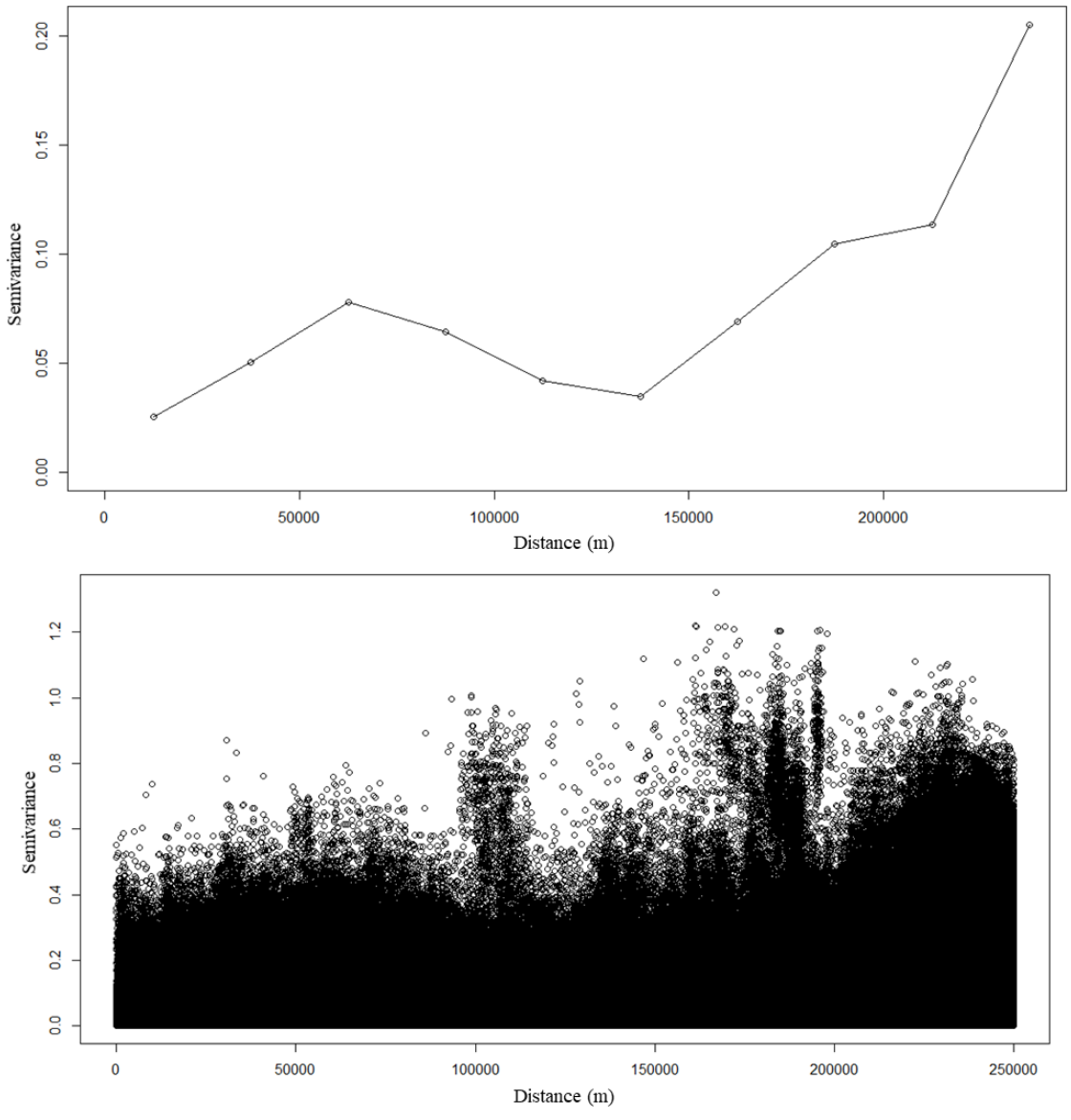

Figure 7: Experimental variogram and variogram cloud for BHT.

3.4.2 Anisotropy

The behavior of the variables' spatial correlation in different directions can be analyzed through variogram maps. The presence of geometric anisotropy in any of the evaluated directions allows confirming the spatial variability of BHT and GG in the sedimentary basins. The variogram map allows for observing anisotropic spatial behaviors for both variables. Directionally, the maps are symmetric, representing the spatial correlation with any axis taken as a reference. In the BHT calculated with TMA, the directional variograms evaluated at 0° (N-S), 45° (NE-SO), 90° (E-O) and 135° (NO-SE), infer that the nugget effect or the nuggets are similar in all four directions. The sills reach lower values at 0° and 45° compared with the other two directions, showing, in turn, a very variable behavior at greater distances. In Figure 8, the variogram maps for BHT are provided.

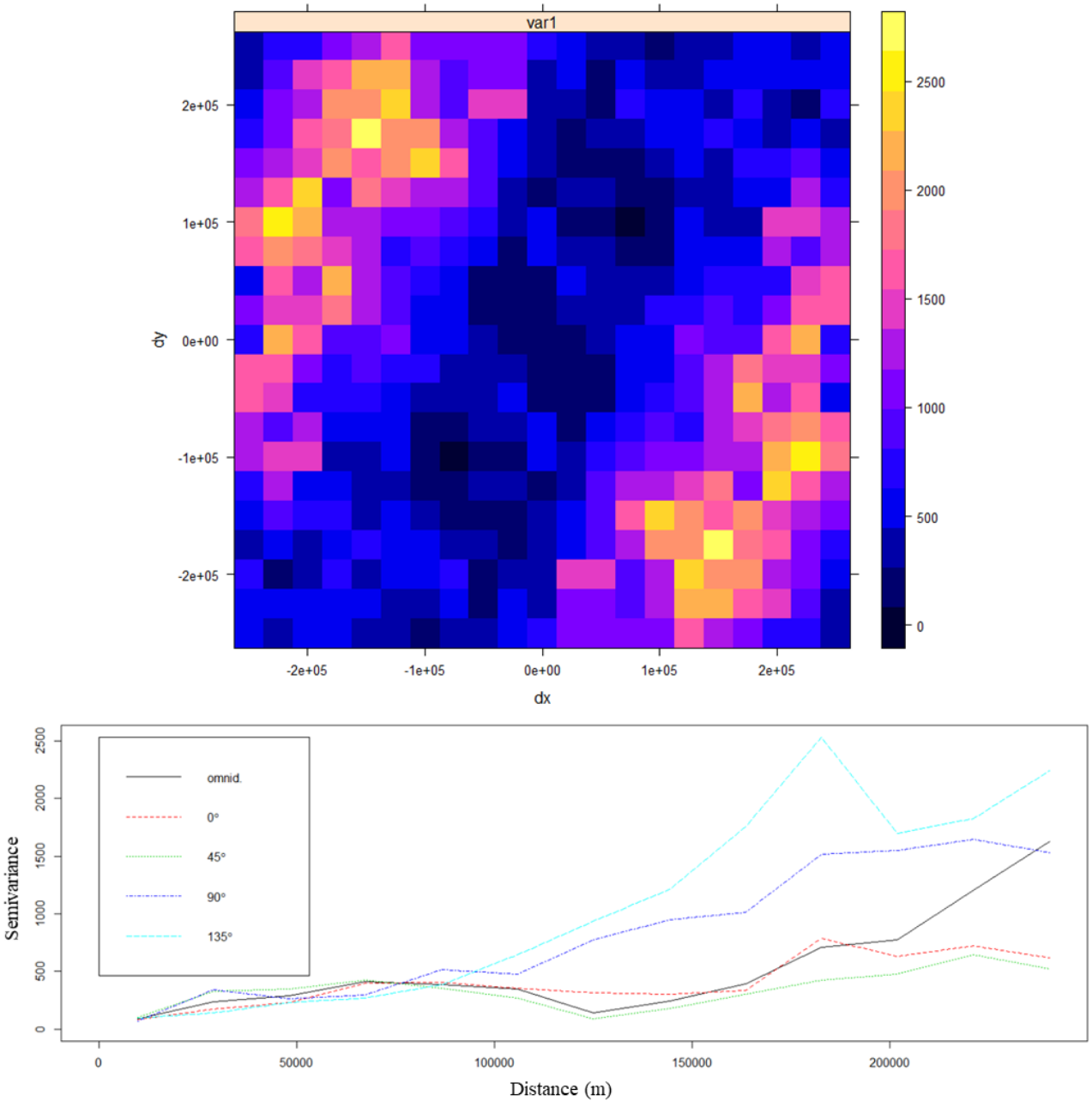

Figure 8: Variogram map and directional variograms for BHT.

3.4.3 Theoretical Variogram

The fit to the experimental variogram was carried out by means of the analytical functions of theoretical variograms using spherical models (sill equal to the range), exponential models (asymptotic sill) and Gaussian models (asymptotic sill with a nugget tending to advance in greater distance from the origin 0). These models are transitional because the estimation of the sill is included in the modeling. In the BHT it is denoted that the theoretical range of the sill is similar up to the range of 175000 m, while for the Gaussian

model it is not reached within the limit of the observation scale of the semivariance. The Gaussian model does not reach a defined sill for the evaluated semivariance. In Figure 9, the models of the theoretical variograms for BHT are characterized. The effect of the spatial correlation in the GG characterized by means of the directional variograms (Figure 9), shows that the geothermal gradients estimated the nugget effect is differentiated for each direction, but similar in its origin. Although the sills are very different from each other, they reach higher values in the N-S and NW-SE directions, corresponding to 0° and 135° respectively, having a greater structural variance. The variogram maps validate the correspondence of the spatially found isotropy levels. Although the nugget is variable in close range, the directional variogram shows that in the 45°, 90° and 135° directions the sills are reached at lower values.

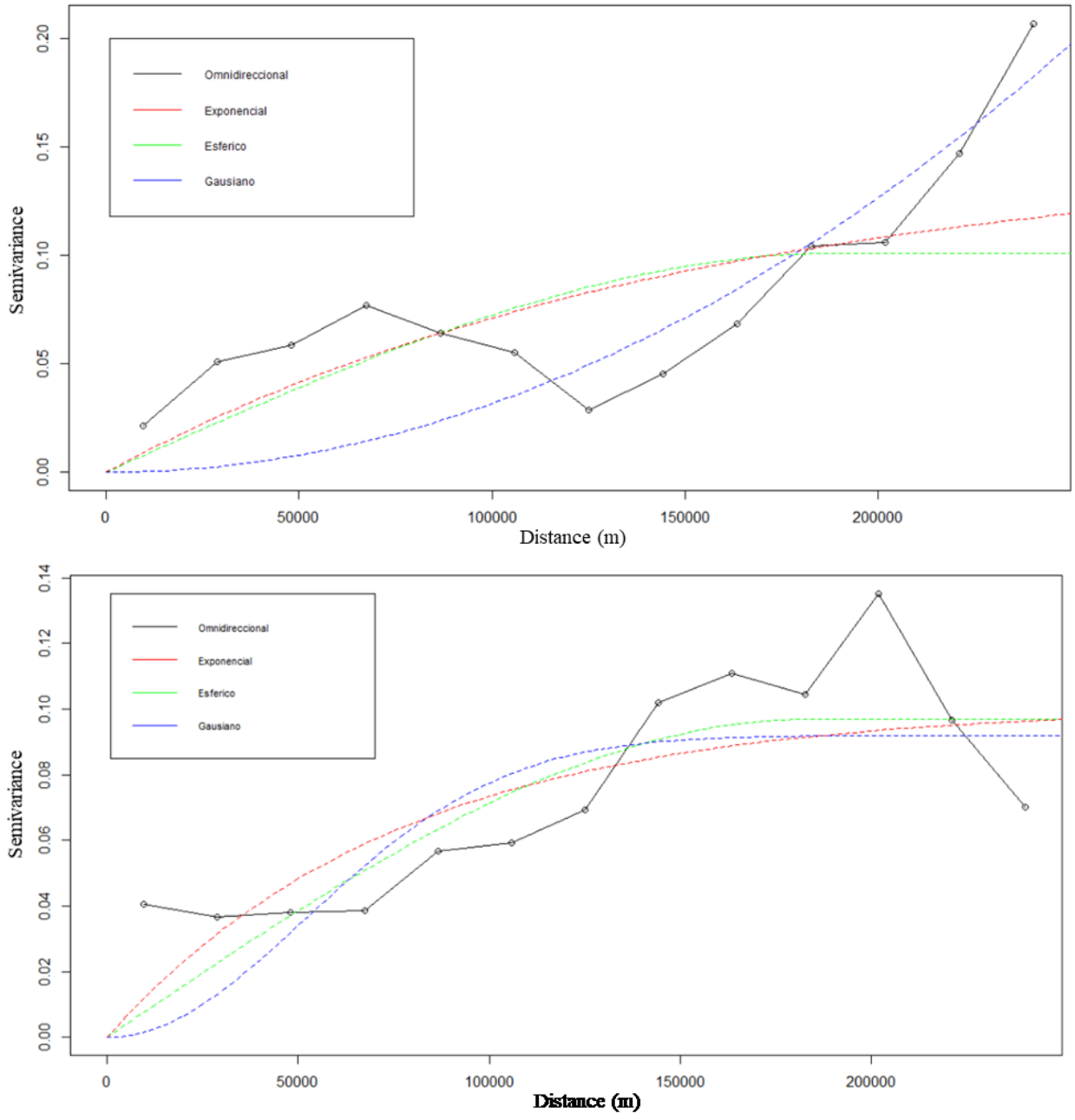

Figure 9: Theoretical variograms (exponential, spherical, and gaussian) for BHT and GG.

3.4.4 Cross-Validation

The cross-validation of the estimates to be predicted allows asserting whether the model of the theoretical variogram correctly describes the spatial dependence of the predicted value close to the real value. In the cross-validation methodology, a value of the variable to be estimated is eliminated, then the adjusted theoretical variogram is calculated where, from this, the predicted value of the eliminated observation is obtained. To select the best theoretical model, two statistical evaluation criteria were taken into account: the Root Mean Square Standardized (RMSS), which must be the same or tend to zero (0). If the RMSS values are greater than 1, the variability of the

predictions is underestimated. On the other hand, if the RMSS values are less than 1, the variability in predictions is overestimated. The other evaluation criterion to be taken into account corresponds to the percentage of data rejected, which should not be greater than 5%. In Table 4, the RMSS statistics are observed for each of the models of the theoretical variograms for the BHT, where it was obtained that the theoretical variogram of the Gaussian model is the one that best represents these variables. The number of accepted observations corresponded to 3303 for BHT and 3285 for GG, with which 0% of rejected data was obtained. When obtaining an RMSS above 1, it follows that the variability of the predictions is underestimated for the BHT and GG.

Table 4: Descriptive measures for BHT and GG.

Variable	Theoretical Variogram Model	Accepted observations number	Percentage of rejected data	RMSS
BHT	Spherical	3303	0%	1.137245
	Exponential			1.155564
	Gaussian			**1.099185**
GG	Spherical	3285	0%	1.167388
	Exponential			1.095529
	Gaussian			**1.030567**

4. SPATIAL REPRESENTATION

The generation of the spatial prediction models was preceded by the exploratory analysis of the data, structural analysis and the spatial representation of the bottom hole temperature and the corrected geothermal gradient. The BHT and GG modeled by spatial prediction were corrected topographically before their representation. The representation of the models of BHT and GG was carried out in 2D and 3D, allowing to determine geometries of the variations of the temperature as a function of the depth.

4.1 Kriging

With the exploratory analysis and the structural analysis applied to the observations, surfaces and volumes of estimation were generated by the ordinary Kriging linear interpolator. This interpolator takes into account the distance between the observations, the weight of the points and the spatial structure of the variable that is represented. The uncertainties of the estimated model are obtained as the standard deviations thereof. All the representations were generated from the best theoretical variogram that adjusts to the experimental variogram of the data: Gaussian model. The most relevant characteristic in the characterization of the estimated model corresponds to the representation grid according to the cell or pixel size. In Figure 10 and Figure 11, the 2D and 3D Kriging models are observed for topographically corrected BHTs.

In 2D Kriging modeling, the cell size was 5000 m (X and Y). For 3D modeling, the grid is composed of voxels, which represent the minimum cubic unit for the generation of volumetric grids. The voxel dimension used in the Kriging 3D modeling was 5000 meters in X, 5000 meters in Y, and 1000 meters in Z. The 2D grids allow relating the positive anomalies of BHT towards the central and northern zone of the Eastern Cordillera basin and the northwestern sector of the Eastern Planes basin (Kellogg et al., 2005). These values of high temperatures coincide with the outcrop of the Paleozoic basement present in the Eastern Planes basin.

The central area of the Middle Magdalena Valley basin (Mojica and Franco, 1990) denotes sectors with high temperatures without anomalies. Towards the south of the basin, medium temperature zones are concentrated. In the western sector of the Valle Medio del Magdalena basin and the eastern sector of the Eastern Planes basin there are negative BHT anomalies, which are associated with the edge effect of the interpolated model. The representations of Kriging 3D modeling are very similar. The anomalies are concentrated in the upper part of the Eastern Cordillera basin, decreasing towards the east at the end of the llanero piedmont in the Eastern Planes basin. Towards the Middle Magdalena Valley basin, average BHT values are concentrated with negative BHT anomalies, linked to the edge effect of the method and interpolation.

For GG, a temperature variation linked with a positive GG anomaly is observed depending on the outcrop of the GG crystalline basement in the West-East direction in the Eastern Planes basin. The central sector of the Eastern Cordillera basin also shows positive GG anomalies in the Southwest-Northeast direction, framed between the Bituma and La Salina Fault System and the Guaicaramo Fault System. In the Middle Magdalena Valley basin, negative anomalies are evidenced with low values of GG, located to the West of the department of Santander. The most northeastern sector of the Llanos Orientales basin concentrates negative anomalies with low GG data. The Middle Magdalena Valley basin associates GG mean values, without negative anomalies. In Kriging 3D models, the same behavior is shown as in 2D modeling. The positive anomalies of high GG are concentrated in the most southeastern part of the Eastern Planes basin and the intermediate zone of the Eastern Cordillera basin (Bachu et al., 1995). A negative anomaly, with low GG observations, is concatenated in the northernmost part of the Eastern Cordillera and Middle Magdalena Valley basins.

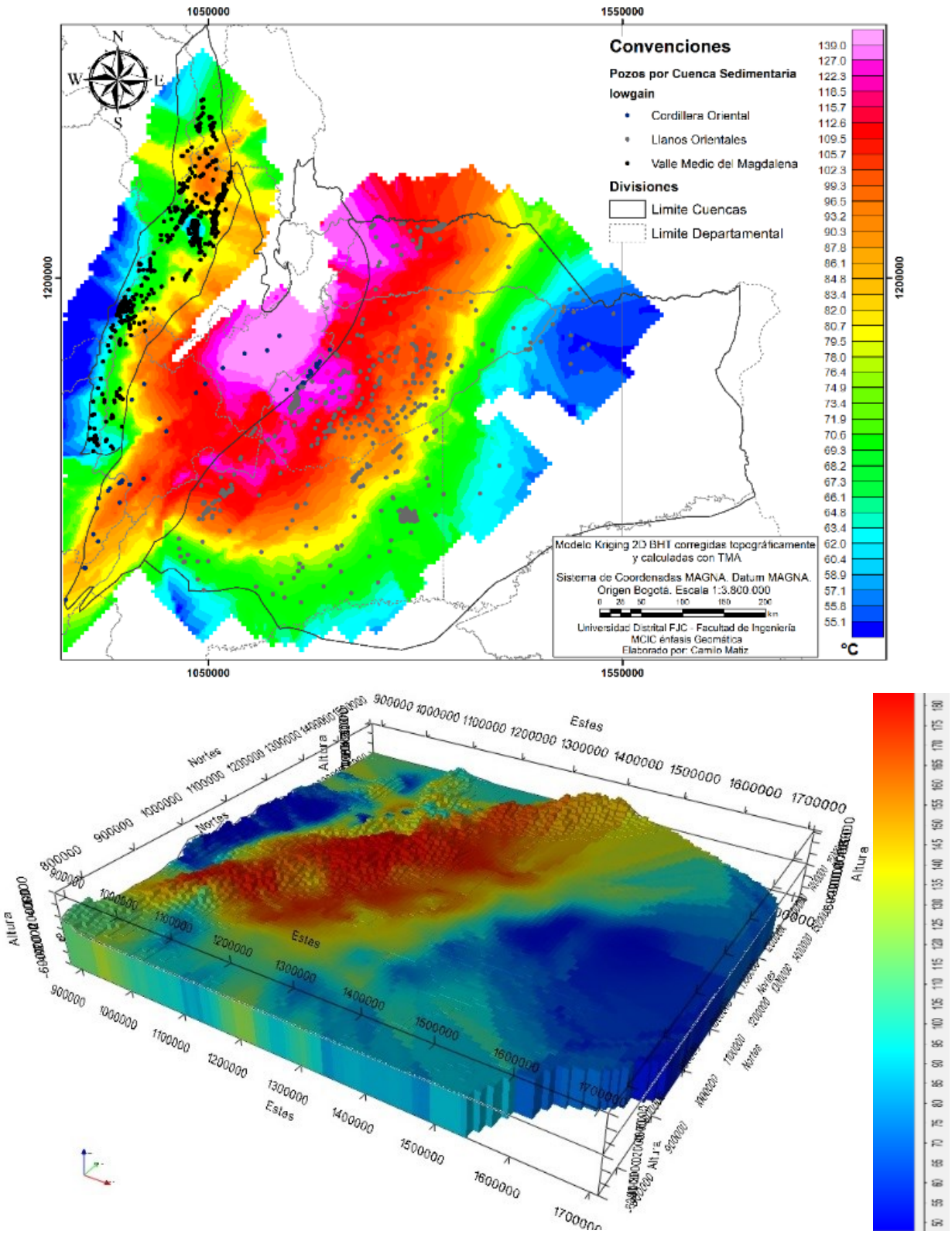

Figure 10: Kriging 2D and 3D for BHT.

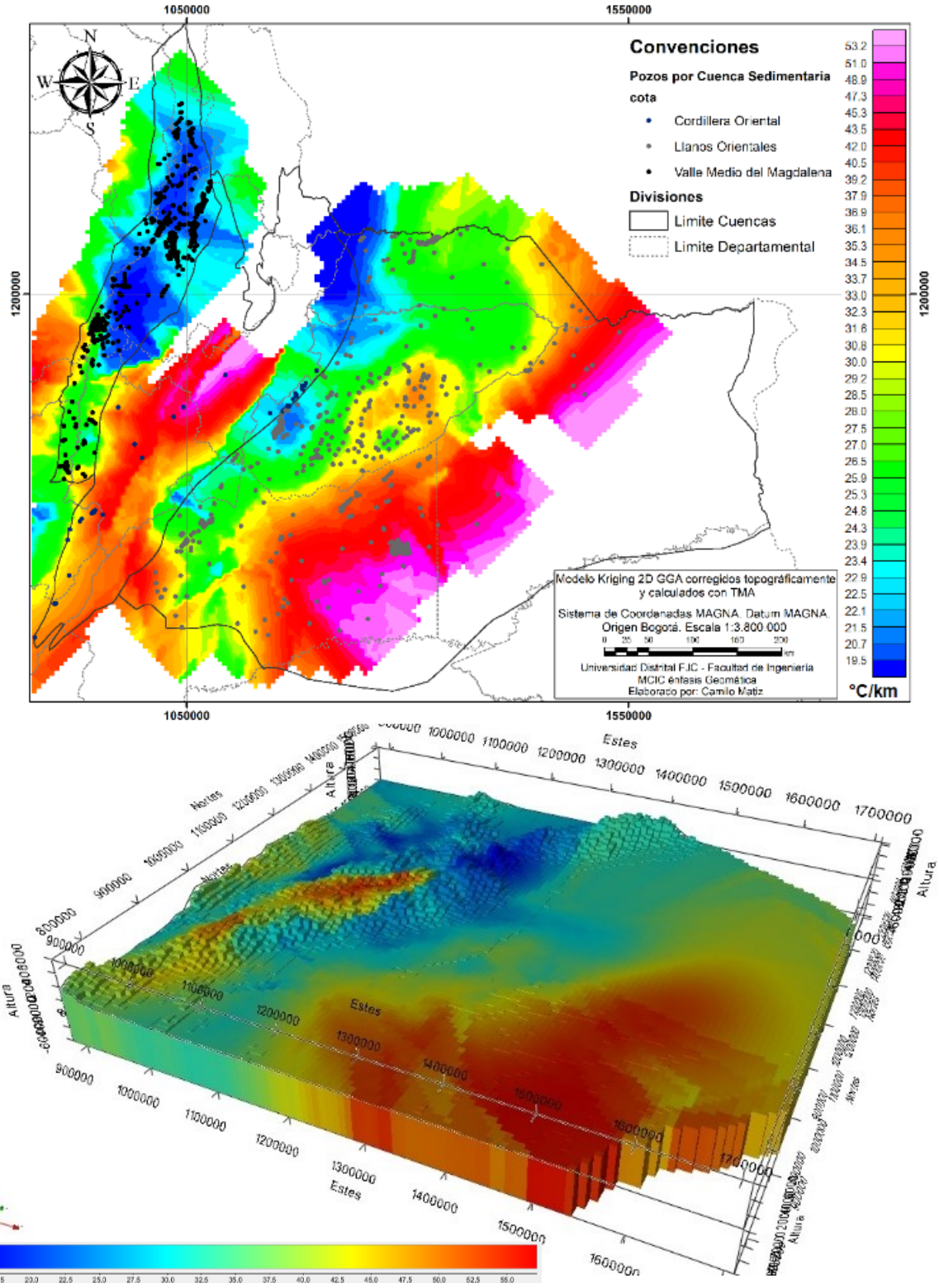

Figure 11: Kriging 2D and 3D for GG.

4.2 Sequential Gaussian Simulation

The results obtained under this method contain the Gaussian anamorphosis transformation, which allows taking the data to a standard Normal distribution (mean = 0 and variance = 1). The stochastic simulation results in many equiprobable surfaces of the BHT and the GG. In the SGS, a random deviation applied to observations was selected based on the normal distribution (Gaussian anamorphosis), according to a uniform random number that represented the probability level of the normal distribution applied as a transformation to

the observations. The SGS uses the Gaussian variogram to model the spatial correlation of the generated 3D grids. The size of each voxel in 3D stochastic modeling corresponded to a volume of 5000 meters in X, 5000 meters in Y, and 1000 meters in Z. The number of simulations applied to the results corresponded to 60 for each simulated variable. The processing times of the 3D grids were approximately 12 hours for 60 simulations. The representation of the resulting voxels was adjusted to the surface topography, which was delimited by the DEM input to the model for the three sedimentary basins to be modeled.

In Figure 12, resulting 3D grids are observed with the stochastic simulation for the BHT and GG. In the vicinity of the Eastern Cordillera basin, a positive anomaly of temperature is denoted, which is characterized by both inputs for the entire extension of the basin, becoming more noticeable in the southwest-northeast direction. For the Eastern Planes basin, it is considered a negative temperature anomaly with an East-West trend. In the Middle Magdalena Valley basin, the negative anomaly is part of the sets of voxels on the western flank of this basin.

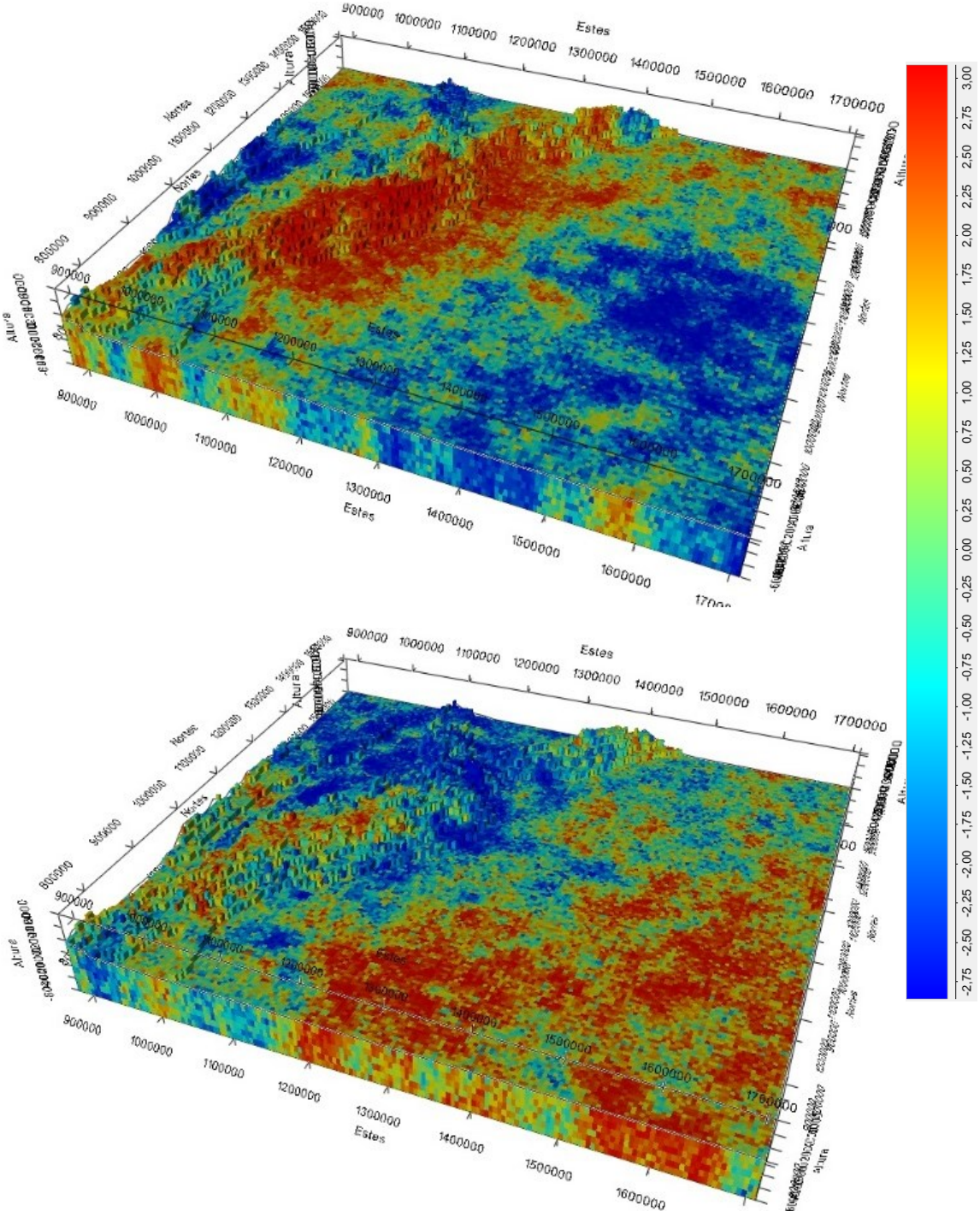

Figure 12: SGC 3D for BHT and GG.

4.3 Inverse Distance Weighting

With the prediction of the surfaces of BHT by means of the Inverse Distance Weighting (IDW) method, a great positive anomaly is observed in the Eastern Cordillera basin. This anomaly is framed within the limits of the piedmont planes in the eastern region of the Eastern Cordillera basin. For the Eastern Planes basin, a transition is observed between the positive anomalies of BHT in the vicinity of the western edge of the basin, which has average temperature values, towards a negative anomaly in the eastern flank of the Eastern Planes basin. In the Middle Magdalena Valley basin, high temperatures are evident towards the northern part of the basin. In the North-South direction, low temperatures are observed throughout the basin. In 3D voxels, a wide correlation is observed between the observations obtained by both estimation methods. The great anomaly of BHT can be seen in most of the extension of the Eastern Cordillera basin, delimited by average temperatures found in the Middle Magdalena Valley basin and low temperatures and a large BHT anomaly towards the northeastern sector of the Eastern Planes basin. Figure 13 and Figure 14 shows the 2D and 3D grids with the BHT and GG values corrected for topography.

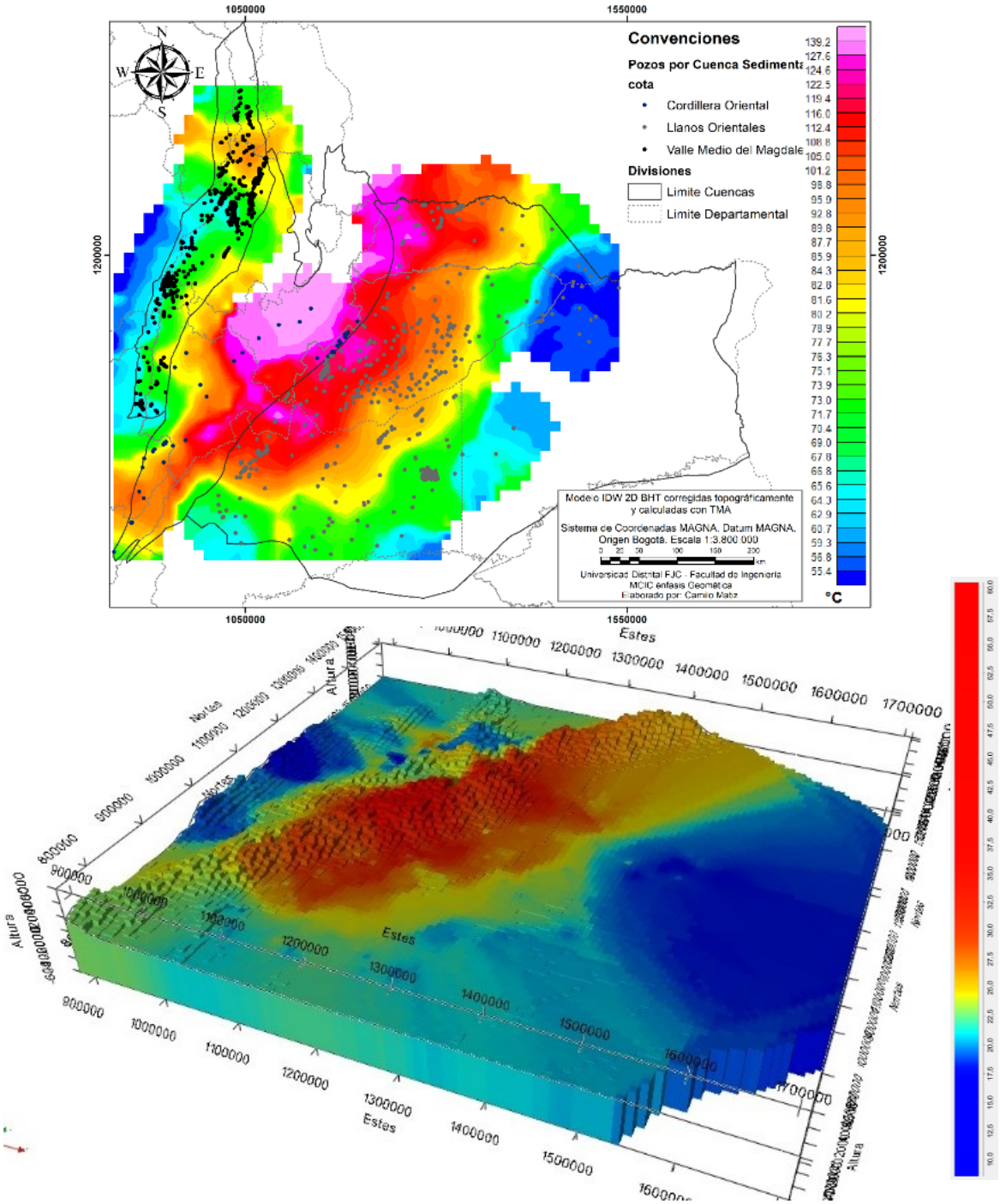

Figure 13: IDW 2D and 3D for BHT.

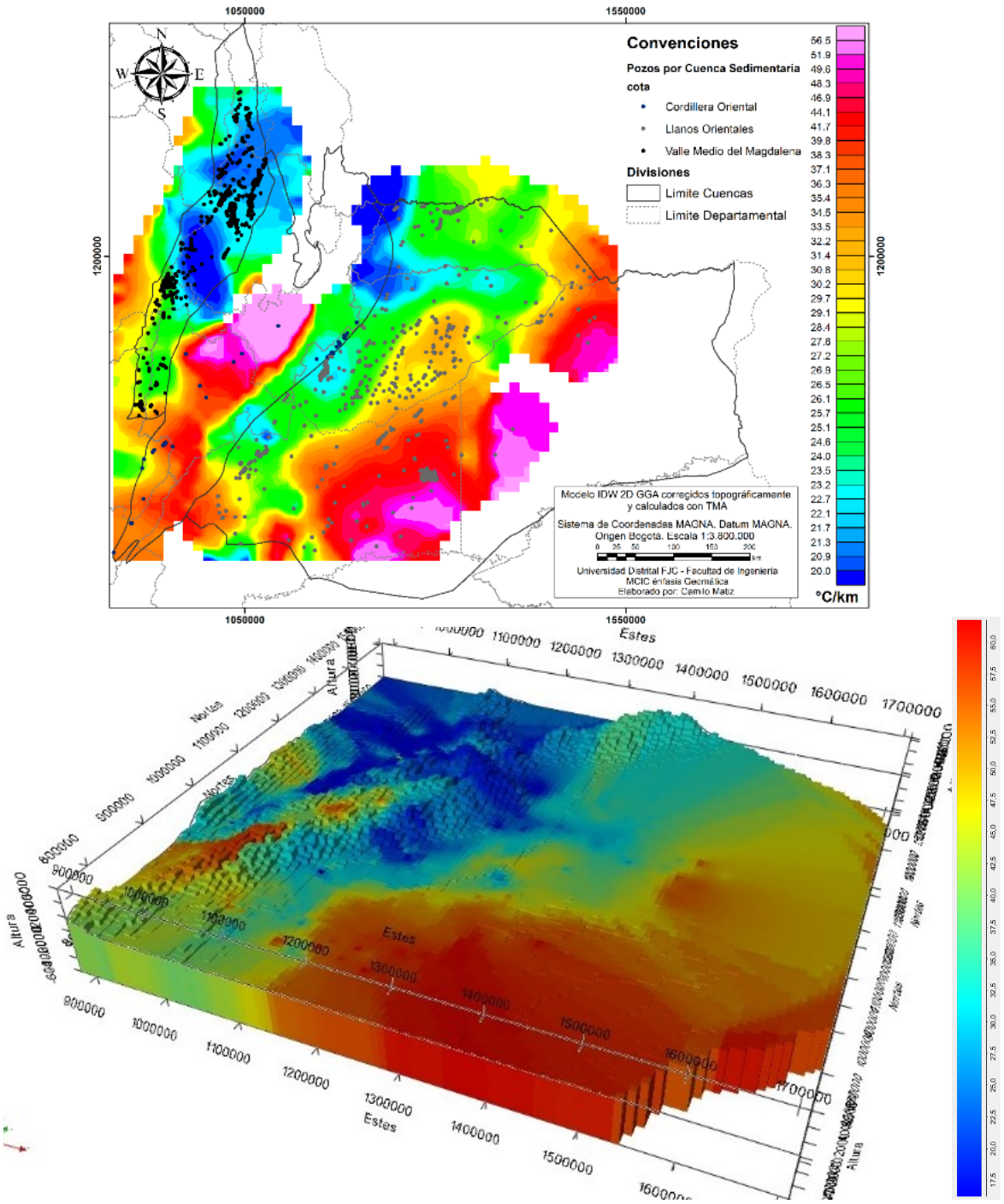

Figure 14: IDW 2D for 3D for GG.

CONCLUSIONS

Given the lack of data directly linked to the geothermal industry, the use of multipurpose information, such as wells in the oil industry, allows the creation of representative scenarios for the nascent geothermal community in Colombia. A robust statistical treatment of the temperature values allows reducing the uncertainty in the way of acquiring data from the oil industry, with which geothermal grids can be calculated and determine the heat flow, which also requires the thermal conductivity of the rock.

The representation of bottom hole temperatures and geothermal gradients calculated by means of data extracted from hydrocarbon wells, allows for characterization of the thermal structure of the sedimentary basins studied. Using geostatistical modeling, it is possible to typify the behavior of the temperature and its variations in relation to the Colombian topography with robust interpolators and algorithms for 3D models. Statistical and spatial analysis allows for recreating that higher temperature values are present in the basin of the Eastern Cordillera, while the highest values of geothermal gradient are located in the Eastern Planes basin and the basin of the

Middle Magdalena Valley (concordant with the location of the oil fields in these two regions). The mean values for the geothermal gradient are located in the Eastern Cordillera basin, influenced by the effect of the topography of the Colombian Andes.

To improve the uncertainty of the data, it is necessary to densify the BHT records, as far as possible with temperature profiles depending on the depth and taken after the drilling is completed, thus completing a temperature profile over time. The reduction of the uncertainty in the estimation of the geothermal gradient can be achieved from the incorporation of temperature profiles that allow to identify changes in the slope, related to vertical variations in thermal conductivity along the lithological column.

REFERENCES

Alfaro, C., Alvarado, I. and Manrique, A.: Heat Flow Evaluation at Eastern Llanos Sedimentary Basin, Colombia, *Proceedings*, World Geothermal Congress, Melbourne, Australia (2015).

Alfaro, C., Alvarado, I. and Manrique Bonilla, A.: Actualización del Mapa Geotérmico de Colombia Fase 2. Mapa preliminar del flujo de calor terrestre en la cuenca de los Llanos Orientales, *Technical Report*, Ingeominas, Bogotá D.C., Colombia (2010).

Alfaro, C., Alvarado, I., Quintero, W., Hamza, V., Vargas, C. and Briceño, L.A.: Mapa preliminar de Gradientes Geotérmicos de Colombia, *Proceedings*, XII Congreso Colombiano de Geología, Sociedad Colombiana de Geología, Bogotá D.C., Colombia (2009).

Álvarez, S., Matiz-León, J.C. and Cárdenas, A.:Modelos digitales batimétricos generados por métodos de interpolación IDW, Kriging, Shepard y B-Spline en el archipiélago de islas del Rosario. *UD y la Geomática*, **5**, (2011), 3–14.

Amezcua, J. and Van Leeuwen, P.J.: Gaussian anamorphosis in the analysis step of the EnKF: a joint state-variable/observation approach. *Tellus A: Dynamic Meteorology and Oceanography*, **66**, (2014), 1–33.

Bachu, S., Ramon, J.C., Villegas, M.E. and Underschultz, J.R.: Geothermal Regime and Thermal History of the Llanos Basin, Colombia, *AAPG Bulletin*, **79**, (1995), 116–129.

Balling, N., Haenel, R., Ungemach, P., Vasseur, G. and Wheildon, J.: Preliminary guidelines for heat flow density determination, *Technical Report*, Commission of the European Communities, Luxemburgo (1981).

Barrero, D., Pardo, A., Vargas, C.A. and Martínez, J.F.: Colombian Sedimentary Basins: Nomenclature, boundaries and Petroleum Geology, a New Proposal, *Technical Report*, Agencia Nacional de Hidrocarburos – ANH, Bogotá D,C., Colombia (2007).

Deming, D.: Application of bottom-hole temperature corrections in geothermal studies, *Geothermics*, **18**, (1989), 775–786.

Deutsch, C. V.: Geostatistical Reservoir Modeling, *Book*, Oxford University Press, New York (2002).

Farr, T., Rosen, P., Caro, E., Crippen, R., Duren, R., Hensley, S., Kobrick, M., Paller, M., Rodriguez, E., Roth, L., Seal, D., Shaffer, S., Shimada, J., Umland, J., Werner, M., Oskin, M., Burbank, D. and Alsdorf, D.: The shuttle radar topography mission, *Reviews of Geophysics*, **45,** (20057), 1–33.

Fortin, M. J. and Dale, M.: Spatial Analysis: A guide for ecologist, *Book*, First edition, Cambridge University Press, Cambridge (2005).

Haining, R.: Spatial Data Analysis. Theory and Practice, *Book*, First edition, Cambridge University Press, Cambridge (2004).

Kellogg, J., Ojeda, G., Duque, H. and Cerón, J.: Crustal structure of the Eastern Cordillera, Colombia, *Proceedings*, 6th International Symposium on Andean Geodynamics - ISAG, Universitat de Barcelona, (2005), 424–427.

Morgan, P. & Scott, P.: New Geothermal Gradient Maps for Colorado´s Sedimentary Basin. GRC Transactions, **38**, (2014), 155-162.

Mojica, J. and Franco, R.: Estructura y Evolución Tectónica del Valle Medio y Superior del Magdalena, Colombia, *Geología Colombiana*, **17**, (1990), 41–64.

Ramírez, G.: Aplicación del Método del Intervalo de Confianza como técnica Geoestadística No Lineal a la Modelación Espacial de variables geotécnicas, *Master's Thesis*, Universidad Nacional, Bogotá D.C., Colombia (2010).

Webster, R. and Oliver, M.A.: Geostatistics for Environmental Scientists, *Book*, Second edition, Jhon Wiley and Sons, Chichester, England (2007)

Westaway, R. and Younger, P.: Accounting for palaeoclimate and topography: a rigorous approach to correction of the British geothermal dataset, *Geothermics*, **48**, (2014), 31–51.